Particle and Fibre Toxicology

RESEARCH

Open Access

Effective density of inhaled environmental and engineered nanoparticles and its impact on the lung deposition and dosimetry

Denisa Lizonova[1], Amogh Nagarkar[2], Philip Demokritou[1] and Georgios A. Kelesidis[1,2*]

Abstract

Background Airborne environmental and engineered nanoparticles (NPs) are inhaled and deposited in the respiratory system. The inhaled dose of such NPs and their deposition location in the lung determines their impact on health. When calculating NP deposition using particle inhalation models, a common approach is to use the bulk material density, ρ_b, rather than the effective density, ρ_{eff}. This neglects though the porous agglomerate structure of NPs and may result in a significant error of their lung-deposited dose and location.

Results Here, the deposition of various environmental NPs (aircraft and diesel black carbon, wood smoke) and engineered NPs (silica, zirconia) in the respiratory system of humans and mice is calculated using the Multiple-Path Particle Dosimetry model accounting for their realistic structure and effective density. This is done by measuring the NP ρ_{eff} which was found to be up to one order of magnitude smaller than ρ_b. Accounting for the realistic ρ_{eff} of NPs reduces their deposited mass in the pulmonary region of the respiratory system up to a factor of two in both human and mouse models. Neglecting the ρ_{eff} of NPs does not alter significantly the distribution of the deposited mass fractions in the human or mouse respiratory tract that are obtained by normalizing the mass deposited at the head, tracheobronchial and pulmonary regions by the total deposited mass. Finally, the total deposited mass fraction derived this way is in excellent agreement with those measured in human studies for diesel black carbon.

Conclusions The doses of inhaled NPs are overestimated by inhalation particle deposition models when the ρ_b is used instead of the real-world effective density which can vary significantly due to the porous agglomerate structure of NPs. So the use of realistic ρ_{eff}, which can be measured as described here, is essential to determine the lung deposition and dosimetry of inhaled NPs and their impact on public health.

Keywords Inhalation, Pulmonary deposition, Engineered nanoparticles, Air pollution, Black carbon, Wood smoke, Effective density

*Correspondence:
Georgios A. Kelesidis
georgios.kelesidis@rutgers.edu
Full list of author information is available at the end of the article

Graphical abstract

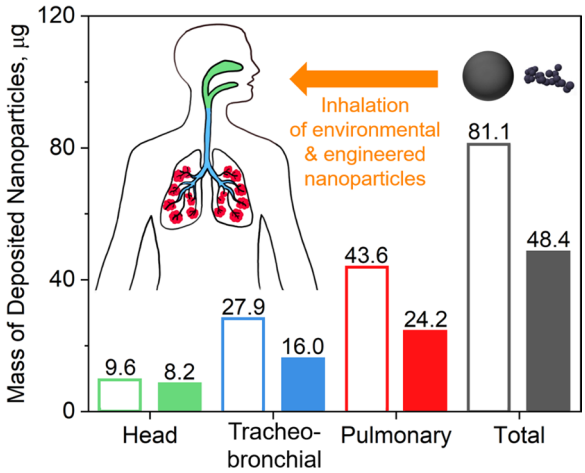

Background

Over the past century, the exposure of humans to airborne environmental and engineered nanoparticles (NPs) has increased dramatically due to air pollution, technological advancements and use in nano-enabled products across the value chain and various industries [1–6]. Such nanoscale particles share unique physicochemical properties that stem from their small size and large surface area, chemistry and reactivity and render them rather toxic to human health [7].

In particular, environmental and engineered NPs have been linked with a variety of pulmonary [8–11], cardiovascular [12–15] and other effects [16–19], even though the underlying mechanisms are still not well understood. It is worth noting that given the continuous rise of air pollution due to climate change [20, 21], as well as the emerging markets for engineered nanomaterials [22], it is essential to get a better understanding of the impact of these NPs on public health.

Most of the (primary) airborne environmental pollutants, such as black carbon (BC) or wood smoke, are emitted from combustion sources, including engines, coal or biomass combustors and wildfires [23–25]. In addition to environmental pollutants, combustion contributes decisively to the formation of nanostructured commodities, including carbon black, silica and titania that are produced in flame reactors [22]. The environmental and engineered NPs formed during these processes coagulate into porous, fractal-like clusters (i.e. agglomerates) [26, 27]. The size of these agglomerates is commonly quantified by their mobility and aerodynamic diameters [28] that vary significantly between materials and combustion sources and processes, as summarized in Table 1. The agglomerate porosity is determined by the effective density, ρ_{eff}, that is defined here as the ratio of the particle mass and equivalent mobility volume and is just a fraction of the material bulk density, ρ_b [28, 29]. The small agglomerate ρ_{eff} affects the gravitational settling, inertial impaction and diffusion of NPs [30] and thus affects their lung deposition and dosimetry.

In nanotoxicology research, both in vivo animal studies as well as in vitro cellular approaches are employed to assess potential toxicological endpoints [31, 32]. Particle lung deposition models such as the Multiple-Path Particle Dosimetry (MPPD) [33, 34] and International Commission on Radiological Protection (ICRP) [35] models, are often used to determine the lung deposited dose using the airborne exposure levels of inhaled NPs. For example, MPPD has been recently used by the authors and others to derive the inhaled dose of ambient particulate matter [36–38], BC [39, 40], wood smoke [41], titania [42], ceria [31, 43], micro- and nanoplastics [44], nano-enabled products [45], printer emitted particles [46, 47] and e-cigarette [48] emissions using ρ_b rather than ρ_{eff}. From the calculated in vivo lung-deposited dose, the in vitro administered dose can also be back-calculated using in vitro particle-kinetic dosimetry models, as described in detail by the authors in previous publications [3, 31, 45, 49, 50]. It should be noted that the effective density for in vitro particle dosimetry is defined as the density of the formed agglomerate in a culture medium [49, 50].

Table 1 Count Median (CMD), Mass Median Mobility (MMMD), Mass Median Aerodynamic (MMAD) diameters, median ρ_{eff} and bulk density, ρ_b, used in the Multiple-Path Particle Dosimetry (MPPD) model for the estimation of deposited NP mass

	Aircraft BC	Diesel BC [65]	Wood Smoke [64]	Silica [70]	Zirconia [71]
CMD, nm	107.8	88.0	159.1	97.3	68.1
MMMD, nm	182.9	349.5	309.5	182.2	132.2
MMAD, nm	83.2	152.8	142.9	65.1	98.8
ρ_{eff}, g/cm^3	0.34	0.28	0.31	0.26	0.68
ρ_b, g/cm^3	1.8	1.8	1.7	2.2	5.7

For simplicity, MPPD is commonly employed using ρ_b which can differ significantly from the ρ_{eff} [31, 38, 39]. This oversimplification may limit though the accuracy of MPPD calculations for various environmental and engineered NPs that form agglomerates with small ρ_{eff} [26]. For example, the total deposited mass of ceria NPs measured in mice was overestimated by MPPD using the ceria ρ_b by up to a factor of two [43]. Similarly, the mass of diesel BC deposited in the human respiratory system obtained using ρ_b (1 g/cm^3) was a factor of two larger than that derived using the measured ρ_{eff} [51].

In this regard, the development and commercialization of aerosol particle mass (APM) analyzers have enabled the accurate measurement of the NP ρ_{eff} [52–55]. During APM measurements, NPs pass through an electric field between two rotating cylindrical electrodes. By adjusting the electric field potential and the rotating electrode angular velocity, the particle mass [52], volume fraction [56] and consequently ρ_{eff} [57] can be measured. It should be noted that APM is well suited for characterization of NP agglomerates, but its accuracy is not well established for elongated particles (e.g. fibers or tubes). For example, the alignment of such particles in an external electric field [58] can result in measurement errors up to 7% [59]. In addition to the APM analyzers, ρ_{eff} can be also measured using electrical low pressure [60] or hypersonic impactors [61] and time-of-flight mass spectrometers [62]. The agglomerate ρ_{eff} can be obtained also in vivo by fitting the MPPD simulations to the measured lung burden [63].

So, APM analyzers have been used to obtain the ρ_{eff} of environmental NPs, including wood smoke [64], BC emissions from diesel [57, 65], gasoline [66, 67] and marine [68] engines, as well as that of engineered nanomaterials (e.g. carbon black [69], silica [70], zirconia [71]). The ρ_{eff} measured that way has facilitated the derivation and validation of advanced computational models [72] for the particle morphology [26], light absorption [73, 74], scattering [75, 76] and even climate impact [77].

Here, APM is used to demonstrate how to measure the ρ_{eff} of model environmental NPs, namely, aircraft-like BC from enclosed jet fuel combustion [78]. The aircraft BC ρ_{eff} obtained here, as well as those of other model NPs obtained from the literature for diesel BC [65], wood smoke [64], silica [70] and zirconia [71] (summarized in Table 1) are used in MPPD to determine the error from dose calculations derived using the commonly used pristine material bulk density. The deposited mass distributions derived using ρ_{eff} are validated with experimental data of human exposure diesel BC emissions [65] and compared to those obtained commonly in the literature using ρ_b.

Results and discussion

Effective density of environmental and engineered NPs

Figure 1 shows the ρ_{eff} measured for various model NPs such as aircraft (squares, this work) or diesel BC (circles [65]), wood smoke (diamonds [64]), silica (triangles [70]) and zirconia (inverse triangles [71]) as a function of their mobility diameter, d_m. The raw ρ_{eff} data presented in Fig. 1 have been obtained for NP agglomerates with distinct d_m. The NP ρ_{eff} decreases up to a factor of about four with increasing d_m due to their

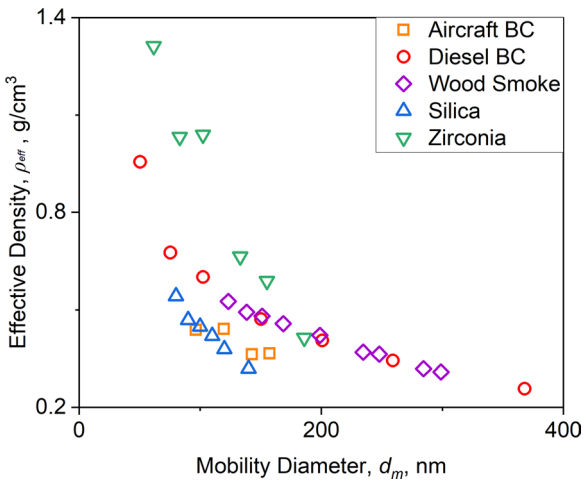

Fig. 1 Effective density, ρ_{eff} as a function of the mobility diameter, d_m, measured for aircraft (squares) or diesel BC (circles [65]), wood smoke (diamonds [64]), silica (triangles [70]) and zirconia (inverse triangles [71]) NPs

fractal-like, agglomerate morphology, which is consistent with theoretical [26] and empirical [79] power laws derived for agglomerates. The ρ_{eff} of zirconia NPs is up to factor of two larger than those of BC, wood smoke and silica due to their larger ρ_b (see Table 1). Similarly, the ρ_{eff} measured here for aircraft BC is up to a factor of 1.4 smaller than that of diesel BC and wood smoke NP agglomerates having the same d_m. The bulk density, ρ_b, is practically the same for aircraft, diesel BC and wood smoke primary particles (Table 1). So, this ρ_{eff} difference can be attributed to the diameter of about 28 nm of diesel BC [65] and wood smoke [64] primary particles that is 50% larger than the diameter of aircraft BC primary particles (12 nm [78]). This is consistent with theoretical power laws showing that ρ_{eff} increases with the primary particle diameter [26]. It is worth noting that the ρ_{eff} presented here for environmental and engineered NPs is up to an order of magnitude smaller than the respective ρ_b.

Using the measured ρ_{eff} along with the entire mobility size distribution, one can obtain the overall NP mass median mobility diameter (MMMD), as well as the mass median aerodynamic diameter (MMAD; see Methods). The latter is essential for the estimation of the NP lung deposition and dose. Even though zirconia NPs have larger ρ_{eff} compared to silica (Fig. 1), their d_m obtained from the entire size distribution is about 30% smaller. This explains the MMMD of silica NPs that is 27% larger than that of zirconia ones. Table 1 summarizes the count median diameter (CMD), MMMD, MMAD, ρ_b and ρ_{eff} of agglomerates having MMAD and MMMD for all NPs used in this study. For example, diesel BC agglomerates with MMAD = 152.8 nm and MMMD = 349.5 nm have ρ_{eff} = 0.28 g/cm^3, which is within the ρ_{eff} = 0.96–0.26 g/cm^3 measured for agglomerates with d_m = 50–368 nm (Fig. 1: circles [65]).

Lung deposition calculations and validation of MPPD dosimetric calculations with human experimental data using ρ_{eff}

Lung deposition of inhaled NPs was simulated using MPPD with realistic ρ_{eff} (Fig. 2) and validated with measurements for the case of diesel BC [65]. The deposited mass fractions derived here by MPPD accounting for the realistic ρ_{eff} of diesel BC are in excellent agreement with the measured ones, validating the MPPD simulations presented in this work. In particular, Fig. 2 compares the mass fraction of deposited diesel BC as a function of its d_m derived by MPPD using ρ_{eff} (line) to those measured from 9 human subjects exposed to the exhaust of a real diesel engine (symbols [65]). These data were obtained using the d_m distributions measured in the inhaled and exhaled air. The ρ_{eff} used in MPPD is varied with d_m using Eq. 2 (see Methods) with

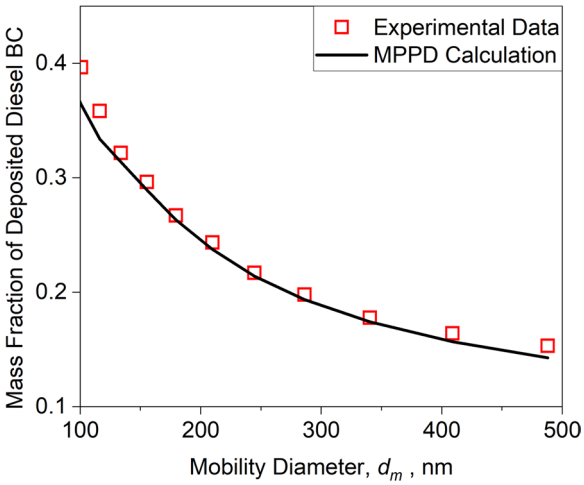

Fig. 2 Mass fraction of deposited diesel BC NPs measured (symbols [65]) or estimated by MPPD (line) as a function of d_m

mass-mobility exponent and prefactor derived by fitting Eq. 2 to the ρ_{eff} measured for diesel BC (see Additional file 1: Table S1). At this size range, the deposition of diesel BC particles by diffusion, inertial impaction and gravitational settling decreases with increasing d_m [80, 81], reducing the total deposited mass fraction.

Impact of ρ_b and ρ_{eff} on lung deposition dose calculations

The deposited mass of environmental and engineered NPs in the respiratory tract of humans (Fig. 3) and mice (Fig. 4) was calculated using the MPPD model with the measured ρ_{eff} (filled bars) or ρ_b (open bars) under the same input parameters. It is worth noting that MPPD, like any other model, has its own limitations and more studies are needed to validate the model for the various conditions and animal models. In humans (Fig. 3), using ρ_b rather than ρ_{eff} results in an overestimation of the total deposited mass by a factor of about two for all environmental and engineered NPs investigated here. Neglecting the realistic agglomerate ρ_{eff} affects also the regional distribution of the deposited mass. For example, using ρ_b in MPPD overestimates the deposited mass of aircraft BC in the head human airways by just 17.1%. However, the deposited aircraft BC mass in the tracheobronchial and pulmonary regions is overestimated using ρ_b by 74.4 and 80.2%, respectively.

The overestimation of the deposited mass of NPs can be attributed to the enhancement of the particle inertial impaction in the TB and pulmonary regions when large ρ_b is used instead of the realistic ρ_{eff} [30]. It should be noted that gravitational settling hardly contributes to the density effects observed here (Additional file 1: Fig. S1). So, the ρ_b is commonly assumed in literature estimations of inhaled NP deposition and dosimetry when

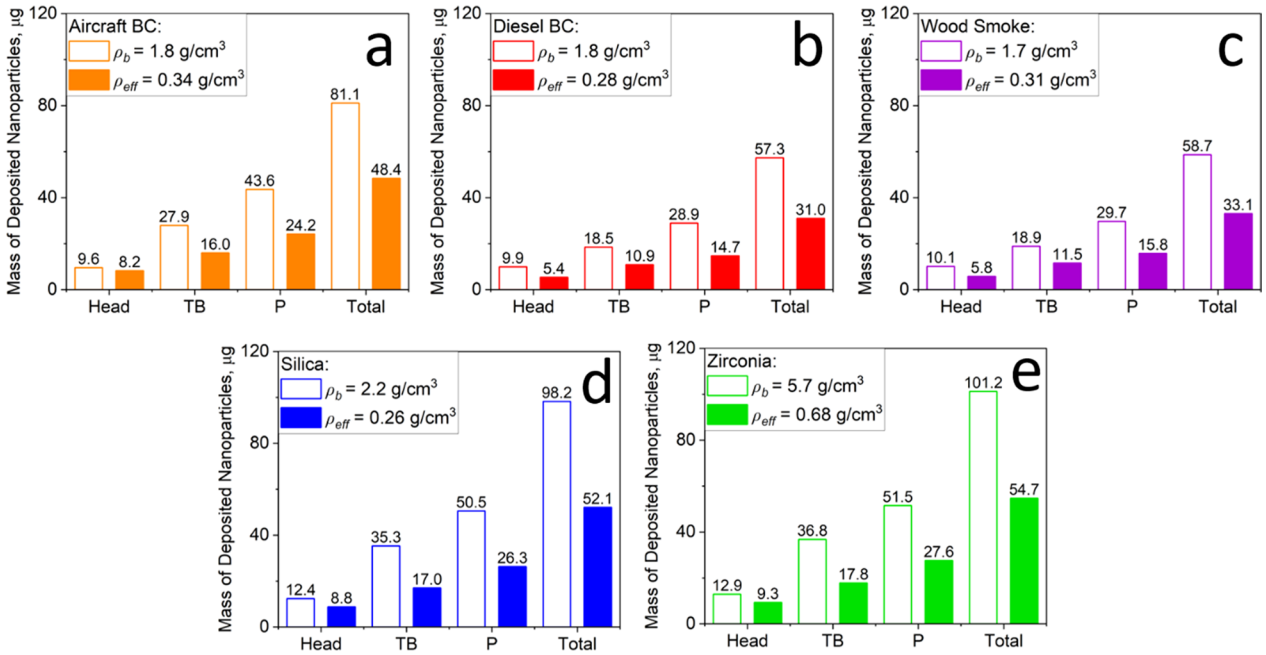

Fig. 3 Mass of deposited NPs in the head, tracheobronchial (TB), pulmonary (P) and total region of the human respiratory tract derived by MPPD for a 40-h exposure to **a** aircraft, **b** diesel BC, **c** wood smoke, **d** silica or **e** zirconia NPs using ρ_b (open bars) or the measured ρ_{eff} (filled bars). The total inhaled dose is 180 µg

the realistic ρ_{eff} is either not known, or for the purpose of simplifying the calculations [38, 39, 43]. This can however lead to significant error in the NP deposition calculation, as is shown here.

Figure 3 shows that most of the particles are deposited in the tracheobronchial (TB) and pulmonary (P) regions of the human respiratory system, where the deposition is governed by diffusion, inertial impaction and

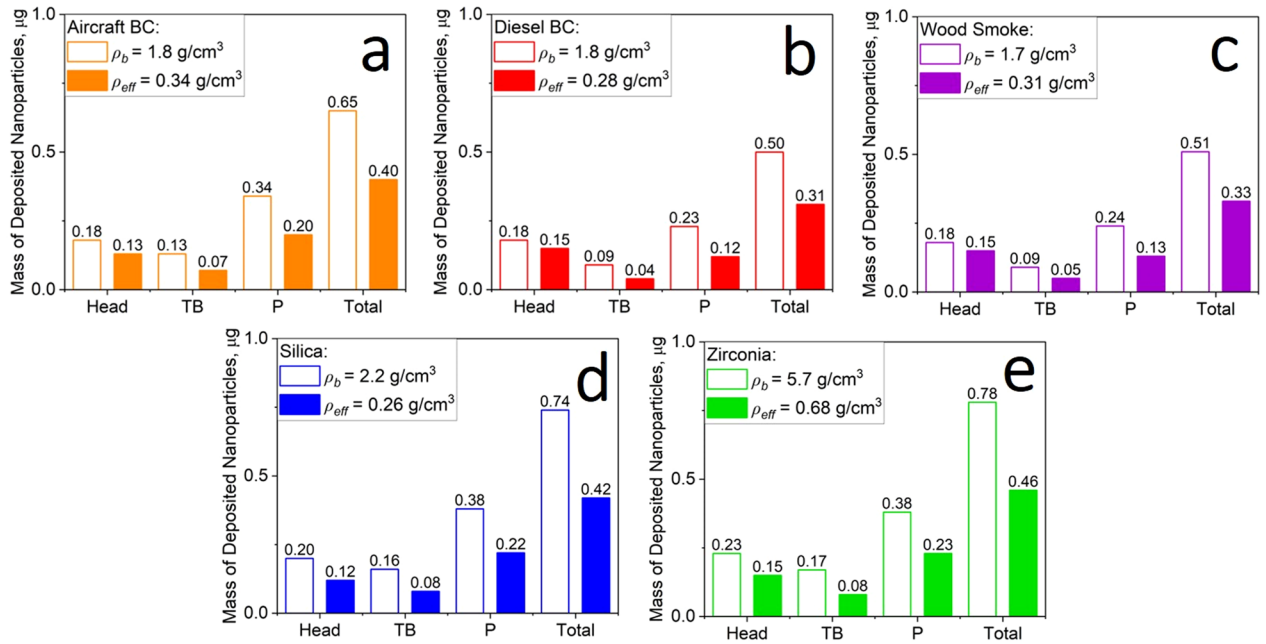

Fig. 4 Mass of deposited NPs in the head, TB, P and total region of the mouse respiratory tract derived by MPPD for a 40-h exposure to **a** aircraft, **b** diesel BC, **c** wood smoke, **d** silica or **e** zirconia NPs using ρ_b (open bars) or the measured ρ_{eff} (filled bars). The total inhaled dose is 1.2 µg

gravitational settling [80–82]. Therefore, the largest deposited mass was obtained for zirconia NPs. These NPs are described by small MMAD compared to those of diesel BC and wood smoke which enhances their deposition by diffusion [80, 82]. Moreover, zirconia NPs are described by high ρ_b and ρ_{eff} compared to those of aircraft BC and silica, which further enhance their inertial impaction [30]. In the head airways of the human respiratory system, only few particles are deposited in all cases, where this is done by an impaction mechanism [80, 81, 83].

The impact of ρ_{eff} on the estimation of the NP deposited dose is similar for both human and mouse models, as shown in Fig. 4. So, neglecting the realistic ρ_{eff} and calculating with ρ_b instead results in an overestimation of the total NP deposited mass in mouse lungs by up to a factor of about two. The largest mass deposited in the TB and pulmonary regions is obtained here for zirconia, consistent with the masses derived for zirconia NPs inhaled by humans (Fig. 3).

In summary, Table 2 shows the total mass of deposited NPs in the human and mouse respiratory tracts derived by MPPD using ρ_b or ρ_{eff}. The overestimation of the total deposited mass by a factor of 1.5–2 obtained here using MPPD with ρ_b is consistent with those reported in literature for engineered [43] and environmental [51] NPs. Clearly, the dose of inhaled engineered and environmental NPs can be overestimated substantially by MPPD using ρ_b, limiting the assessment of their impact on pulmonary [8, 9] and cardiovascular diseases [12–15].

Furthermore, Fig. 5 shows the distribution across the respiratory system of the deposited mass fraction of inhaled aircraft BC NPs by humans (a) and mice (b) derived here by MPPD using ρ_b (open bars) or ρ_{eff} (filled bars). The deposited mass fraction is obtained by normalizing the mass deposited in the head, TB or pulmonary region of the tract with respect to the total deposited mass. Accounting for the realistic ρ_{eff} of aircraft BC reduces its inertial impaction in all regions of the human or mouse respiratory tract and does not alter significantly the distribution of the deposited mass fractions. The distributions of the deposited mass fractions derived here for diesel BC, wood smoke, silica and zirconia are similar to those obtained for aircraft BC and presented in Additional file 1: Fig. S2.

Conclusions

In sum, the error in NP lung deposition dose calculations which is derived using the ρ_b rather than the actual ρ_{eff} of NPs was assessed here using a variety of model environmental and engineered NPs. As shown, the ρ_{eff} measured here for aircraft black carbon (BC) NPs using an APM is one order of magnitude smaller than ρ_b and follows closely those measured in literature for diesel BC

Table 2 Total mass of deposited aircraft, diesel BC, wood smoke, silica and zirconia NPs in the human and mouse respiratory tracts derived by MPPD using ρ_b or ρ_{eff}. The total inhaled dose is 180 and 1.2 µg for human and mouse, respectively

Total mass of deposited NPs, µg	Aircraft BC		Diesel BC		Wood smoke		Silica		Zirconia	
	Human	Mouse	Human	Mouse	Human	Mouse	Human	Mouse	Human	Mouse
MPPD using ρ_b	81.1	0.65	57.3	0.50	58.7	0.51	98.2	0.74	101.2	0.78
MPPD using ρ_{eff}	48.4	0.40	31.0	0.31	33.1	0.33	52.1	0.42	54.7	0.46

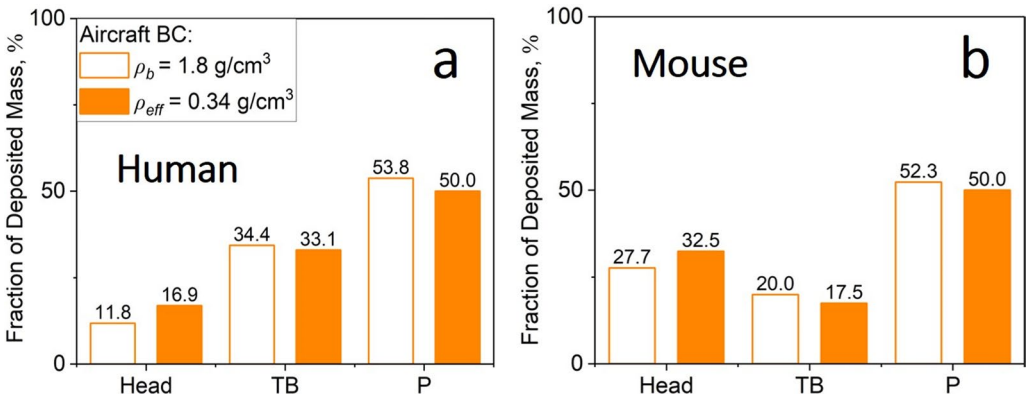

Fig. 5 Fraction of deposited mass in the head, TB and P region of the **a** human and **b** mouse respiratory tract derived by MPPD for a 40-h exposure to aircraft BC using ρ_b (open bars) or the measured ρ_{eff} (filled bars)

[65], wood smoke [64], silica [70] and zirconia [71]. It was shown that the MPPD-derived mass fraction of diesel BC NPs deposited in the human lungs is in excellent agreement with experimental data [65], validating the importance of using the realistic ρ_{eff} rather than the commonly used ρ_b.

More importantly, it was shown that using ρ_b and neglecting the realistic porous structure of environmental and engineered NPs results in an overestimation of their deposited mass by a factor of about two. This can be attributed to the NP inertial impaction that is overestimated by MPPD using ρ_b instead of ρ_{eff}. This may explain similar discrepancies reported in literature for ceria [43] and diesel BC [51] NPs and highlights the role of ρ_{eff} in the modeling of lung deposition of NPs. So, the use of realistic ρ_{eff} in lung deposition models is essential to determine the dose of inhaled NPs, enabling the accurate assessment of their impact on human health.

Methods

Synthesis of aircraft-like BC NPs and measurement of their size and effective density

Aircraft-like BC NPs were generated here by enclosed spray combustion of jet A fuel at an effective equivalence ratio of 1.77 [78]. The morphology, composition, nanostructure and primary particle size distribution of the BC NPs emitted by the present reactor (Additional file 1: Fig. S3) are in excellent agreement with those measured from real aircraft engines [84, 85]. So, the aircraft-like BC produced here was sampled using a straight tube and rapidly diluted by a factor of about 65 [71]. The diluted aerosol was directed to a scanning mobility particle sizer (SMPS) made of a differential mobility analyzer (Model 3081, TSI Inc.) coupled with a condensation particle counter (Model 3775, TSI Inc.) [71]. The CMD and MMMD of the d_m distribution obtained by SMPS are given in Table 1. The mass, m, of the sampled aerosol was also measured by interfacing an aerosol particle mass (APM, Model APM-3600, Kanomax) analyzer with the SMPS [86]. That way, the ρ_{eff} can be derived from first principles [28]:

$$\rho_{eff} = \frac{m}{\frac{\pi}{6} d_m^3} \tag{1}$$

The NP agglomerate ρ_{eff} measured this way decreases with d_m based on a power law [87]:

$$\rho_{eff} = \frac{6k}{\pi} d_m^{D_{fm}-3} \tag{2}$$

where k and D_{fm} are the mass-mobility prefactor and exponent, respectively. The NP agglomerate k and D_{fm} were derived by fitting Eq. 2 to the data shown in Fig. 1 (Additional file 1: Table S1). So, ρ_{eff} can be estimated for any d_m using Eq. 2 and the fitted k and D_{fm}. MMAD was derived based on the measured MMMD and ρ_{eff} [87, 88]:

$$\mathrm{MMAD} = \mathrm{MMMD}\sqrt{\frac{\rho_{eff} C_C(\mathrm{MMMD})}{\rho_o C_C(\mathrm{MMAD})}} \tag{3}$$

where $\rho_o = 1$ g/cm^3 is the unitary density and C_C is the Cunningham slip correction factor [80]:

$$C_C(d) = 1 + \frac{2\lambda}{d}(1.257 + 0.4\exp(-0.78d/\lambda) \tag{4}$$

where d = MMMD or MMAD and $\lambda = 66$ nm is the gas mean free path at room temperature [80]. The MMAD was obtained for aircraft BC NPs generated here, as well as for the diesel BC [65], wood smoke [64], silica [70] and zirconia [71] NPs using ρ_{eff} and d_m distribution data available in the literature (Table 1).

Simulation of NP deposition in the respiratory system using MPPD model

The MPPD model (V3.04) was used here to simulate the deposition of inhaled engineered and environmental NPs in the lung airway from the head to the alveolar region [33, 34, 89, 90]. MPPD calculations for humans were done using the Yeh/Schum symmetric model [91] with a functional residual capacity of 3300 mL and head volume of 50 mL [92]. The nasal respiratory rate (RR) was set to 12 breaths/minute, the tidal volume (TV) to 625 mL and the inspiratory fraction to 0.5 [92]. MPPD calculations were also done for mice using the mouse BALB/c model [33] with body weight of 30 g [93]. The RR of 224 breaths/min and TV of 0.22 mL derived for mice using the allometric scaling equations of Guyton et al. [94] and Piccione et al. [95], respectively, were used for input into MPPD. The functional residual capacity (FRC) of 0.3 mL was used to be consistent with the measured range of 0.20–0.43 mL [96]. The upper respiratory tract (URT) volume of 0.0322 mL used here is the default MPPD value, which is based on experimental measurements [93] and is commonly utilized in MPPD simulations [97, 98]. Both humans and mice were assumed to be exposed to a particle concentration of 0.01 mg/m^3 at "upright" and "on stomach" body orientations, respectively. The latter is consistent with in vivo conscious animal studies [99]. The mass concentration of 0.01 mg/m^3 is the proposed $PM_{2.5}$ limit by United States Environmental Protection Agency (EPA) [100]. It should be noted that $PM_{2.5}$ contains larger particles than those investigated here that are largely contained in the $PM_{0.1}$ aerodynamic

size fraction. In this regard, the mass concentration of $PM_{0.1}$ emissions from the combustion sources investigated here are often much larger than the EPA $PM_{2.5}$ limit used here. For example, mass concentrations of 3.3–26, 0.6–0.8 and 0.004–0.5 mg/m^3 have been measured from pinewood [24], diesel [101], and jet fuel [102] combustion, respectively. The MPPD parameters are summarized in Additional file 1: Table S2. The inhaled NPs were assumed to be monodisperse having the measured MMAD and ρ_{eff} (Table 1) or the constant bulk densities, $\rho_b = 1.8$, 1.7, 2.2 and 5.7 g/cm^3 for BC, wood smoke, silica and zirconia, respectively. The wood smoke ρ_b is obtained based on the measured organic carbon content and empirical ρ_b relations [74]. The deposited mass is calculated from the MPPD-derived regional deposited mass rate per minute (μg/min) by integrating over 40 h of exposure (equivalent to 8 h per day, 5 days per week), as previously described by Bitounis et al. [10]. It is worth noting that MPPD, despite its wide use in the nanotoxicology domain, has its own limitations (like any other available inhalation dosimetry model) and further validation studies related to its proposed conditions and animal models will be useful in advancing the dosimetry field.

The impact of the ρ_{eff} variation with d_m on the MPPD calculations was also investigated here. To this end, the lung deposition of aircraft BC was simulated assuming monodisperse particles with MMAD, as well as accounting for their polydispersity by discretizing their d_m distribution into 10 bins (Additional file 1: Table S3) using Eq. 2 with k, D_{fm} derived by fitting Eq. 2 to the ρ_{eff} measured for aircraft BC (Additional file 1: Table S1). Accounting for the geometric standard deviation of the mobility size distribution, as well as for the ρ_{eff} variation with d_m decreased the total deposited mass just by 6% (Additional file 1: Fig. S4). Therefore, the lung deposition of inhaled NPs can be estimated rather accurately neglecting their polydispersity.

Abbreviations

APM	Aerosol particle mass analyzer
BC	Black carbon
CMD	Count median diameter
EPA	United States Environmental Protection Agency
ICRP	International Commission on Radiological Protection
MMAD	Mass median aerodynamic diameter
MMMD	Mass median mobility diameter
MPPD	Multiple-path particle dosimetry model
NPs	Nanoparticles
P	Pulmonary
PM	Particulate matter
SMPS	Scanning mobility particle sizer
TB	Tracheobronchial

List of symbols

C_C	Cunningham slip correction factor
d	Diameter (nm)
d_m	Mobility diameter (nm)
m	Mass (kg)

Greek letters

λ	Gas mean free path (nm)
ρ_o	Unitary density (1 g/cm^3)
ρ_b	Bulk density (g/cm^3)
ρ_{eff}	Effective density (g/cm^3)

Supplementary Information

The online version contains supplementary material available at https://doi.org/10.1186/s12989-024-00567-9.

Additional file 1: Supplementary Information including **Figure S1.** Mass of deposited NPs in the head, TB, P and total region of the human respiratory tract derived by MPPD for a 40-h exposure to aircraft black carbon using the bulk or the measured effective density and gravitational constants of 9.81 (**a**) or 0 m/s (**b**); **Figure S2.** Fraction of deposited mass in the head, TB and P region of the human and mouse respiratory tract derived by MPPD for a 40-h exposure to **a**-**b** diesel BC, **c**-**d** woodsmoke, **e**-**f** silica and **g**-**h** zirconia using the bulk or the measured effective density; **Figure S3.** Schematic of the experimental set up for preparation of aircraft black carbon nanoparticles from enclosed spray combustion of jet fuel; **Figure S4.** Mass of deposited aircraft black carbon nanoparticles in the human respiratory tract derived by MPPD for a 40-h exposure based on one bin or the mass-weighted average of 10 bins used to discretize the mobility size distribution of aircraft black carbon; **Table S1.** Summary of the massmobility prefactor and exponent derived by fitting Eq. 2 to the measured effective densities shown in Fig. 1; **Table S2.** Summary of parameters used for the particle deposition calculations for humans and mice using the MPPD model (V3.04); **Table S3.** Count Median Diameter, Mass Median Aerodynamic Diameter, bin median effective density and mass fraction of aircraft black carbon having a mobility size distribution discretized into 10 bins.

Acknowledgements
Not applicable.

Author contributions
DL: MPPD calculations, manuscript preparation, preparation of figures. AN: effective density measurements. PD: conceptualization, funding, manuscript preparation. GAK: conceptualization, research project supervision, manuscript preparation, funding.

Funding
This research was funded by EPHEDRA grant no. 1R01ES033250-01A1, CEED NIEHS Center grant no. P30 ES005022, and in part by the Particle Technology Laboratory, ETH Zurich and the Swiss National Science Foundation (200020_182668, 250320_163243 and 206021_170729).

Availability of data and materials
All data generated or analyzed during this study are included in this published article and its supplementary information file.

Declarations

Ethics approval and consent to participate
Not applicable.

Consent for publication
Not applicable.

Competing interests
Authors declare that they have no competing interests.

Author details
[1]Nanoscience and Advanced Materials Center (NAMC), Environmental and Occupational Health Science Institute, School of Public Health, Rutgers, The State University of New Jersey, 170 Frelinghuysen Road, Piscataway, NJ

08854, USA. [2]Particle Technology Laboratory, Department of Mechanical and Process Engineering, Institute of Process Engineering, ETH Zürich, Sonneggstrasse 3, 8092 Zurich, Switzerland.

Received: 1 September 2023 Accepted: 7 February 2024
Published online: 17 February 2024

References

1. Sotiriou GA, Singh D, Zhang F, Chalbot M-CG, Spielman-Sun E, Hoering L, Kavouras IG, Lowry GV, Wohlleben W, Demokritou P. Thermal decomposition of nano-enabled thermoplastics: possible environmental health and safety implications. J Hazard Mater. 2016;305:87–95.
2. Singh D, Marrocco A, Wohlleben W, Park H-R, Diwadkar AR, Himes BE, Lu Q, Christiani DC, Demokritou P. Release of particulate matter from nano-enabled building materials (NEBMs) across their lifecycle: potential occupational health and safety implications. J Hazard Mater. 2022;422:126771.
3. Pirela SV, Miousse IR, Lu X, Castranova V, Thomas T, Qian Y, Bello D, Kobzik L, Koturbash I, Demokritou P. Effects of laser printer–emitted engineered nanoparticles on cytotoxicity, chemokine expression, reactive oxygen species, DNA methylation, and DNA damage: a comprehensive in vitro analysis in human small airway epithelial cells, macrophages, and lymphoblasts. Environ Health Perspect. 2016;124:210–9.
4. Pirela SV, Sotiriou GA, Bello D, Shafer M, Bunker KL, Castranova V, Thomas T, Demokritou P. Consumer exposures to laser printer-emitted engineered nanoparticles: a case study of life-cycle implications from nano-enabled products. Nanotoxicology. 2015;9:760–8.
5. Sohal IS, O'Fallon KS, Gaines P, Demokritou P, Bello D. Ingested engineered nanomaterials: state of science in nanotoxicity testing and future research needs. Part Fibre Toxicol. 2018;15:1–31.
6. Oberdörster G, Oberdörster E, Oberdörster J. Nanotoxicology: an emerging discipline evolving from studies of ultrafine particles. Environ Health Perspect. 2005;113:823–39.
7. Oberdörster G, Maynard A, Donaldson K, Castranova V, Fitzpatrick J, Ausman K, Carter J, Karn B, Kreyling W, Lai D. Principles for characterizing the potential human health effects from exposure to nanomaterials: elements of a screening strategy. Part Fibre Toxicol. 2005;2:1–35.
8. Sager TM, Castranova V. Surface area of particle administered versus mass in determining the pulmonary toxicity of ultrafine and fine carbon black: comparison to ultrafine titanium dioxide. Part Fibre Toxicol. 2009;6:1–12.
9. Choi HS, Ashitate Y, Lee JH, Kim SH, Matsui A, Insin N, Bawendi MG, Semmler-Behnke M, Frangioni JV, Tsuda A. Rapid translocation of nanoparticles from the lung airspaces to the body. Nat Biotechnol. 2010;28:1300–3.
10. Bitounis D, Huang Q, Toprani SM, Setyawati MI, Oliveira N, Wu Z, Tay CY, Ng KW, Nagel ZD, Demokritou P. Printer center nanoparticles alter the DNA repair capacity of human bronchial airway epithelial cells. NanoImpact. 2022;25:100379.
11. Ardona HAM, Zimmerman JF, Shani K, Kim S-H, Eweje F, Bitounis D, Parviz D, Casalino E, Strano M, Demokritou P. Differential modulation of endothelial cytoplasmic protrusions after exposure to graphene-family nanomaterials. NanoImpact. 2022;26:100401.
12. Stampfl A, Maier M, Radykewicz R, Reitmeir P, Gottlicher M, Niessner R. Langendorff heart: a model system to study cardiovascular effects of engineered nanoparticles. ACS Nano. 2011;5:5345–53.
13. Mills NL, Donaldson K, Hadoke PW, Boon NA, MacNee W, Cassee FR, Sandström T, Blomberg A, Newby DE. Adverse cardiovascular effects of air pollution. Nat Clin Pract Cardiovasc Med. 2009;6:36–44.
14. Carll AP, Salatini R, Pirela SV, Wang Y, Xie Z, Lorkiewicz P, Naeem N, Qian Y, Castranova V, Godleski JJ. Inhalation of printer-emitted particles impairs cardiac conduction, hemodynamics, and autonomic regulation and induces arrhythmia and electrical remodeling in rats. Part Fibre Toxicol. 2020;17:1–21.
15. Sotiriou GA, Diaz E, Long MS, Godleski J, Brain J, Pratsinis SE, Demokritou P. A novel platform for pulmonary and cardiovascular toxicological characterization of inhaled engineered nanomaterials. Nanotoxicology. 2012;6:680–90.
16. DeLoid GM, Cao X, Coreas R, Bitounis D, Singh D, Zhong W, Demokritou P. Incineration-generated polyethylene micro-nanoplastics increase triglyceride lipolysis and absorption in an in vitro small intestinal epithelium model. Environ Sci Technol. 2022;56:12288–97.
17. Cao X, Khare S, DeLoid GM, Gokulan K, Demokritou P. Co-exposure to boscalid and TiO_2 (E171) or SiO_2 (E551) downregulates cell junction gene expression in small intestinal epithelium cellular model and increases pesticide translocation. NanoImpact. 2021;22:100306.
18. Toprani SM, Bitounis D, Huang Q, Oliveira N, Ng KW, Tay CY, Nagel ZD, Demokritou P. High-throughput screening platform for nanoparticle-mediated alterations of DNA repair capacity. ACS Nano. 2021;15:4728–46.
19. Bazina L, Bitounis D, Cao X, DeLoid GM, Parviz D, Strano MS, Lin H-YG, Bell DC, Thrall BD, Demokritou P. Biotransformations and cytotoxicity of graphene and inorganic two-dimensional nanomaterials using simulated digestions coupled with a triculture in vitro model of the human gastrointestinal epithelium. Environ Sci Nano. 2021;8:3233–49.
20. Jaffe DA, O'Neill SM, Larkin NK, Holder AL, Peterson DL, Halofsky JE, Rappold AG. Wildfire and prescribed burning impacts on air quality in the United States. J Air Waste Manag Assoc. 2020;70:583–615.
21. Jacob DJ, Winner DA. Effect of climate change on air quality. Atmospheric Environ. 2009;43:51–63.
22. Kelesidis GA, Pratsinis SE. A perspective on gas-phase synthesis of nanomaterials: process design, impact and outlook. Chem Eng J. 2021;421:129884.
23. Bond TC, Doherty SJ, Fahey DW, Forster PM, Berntsen T, DeAngelo BJ, Flanner MG, Ghan S, Kärcher B, Koch D. Bounding the role of black carbon in the climate system: a scientific assessment. J Geophys Res Atmos. 2013;118:5380–552.
24. Singh D, Tassew DD, Nelson J, Chalbot M-CG, Kavouras IG, Demokritou P, Tesfaigzi Y. Development of an integrated platform to assess the physicochemical and toxicological properties of wood combustion particulate matter. Chem Res Toxicol. 2022;35:1541–57.
25. Singh D, Tassew DD, Nelson J, Chalbot M-CG, Kavouras IG, Tesfaigzi Y, Demokritou P. Physicochemical and toxicological properties of wood smoke particulate matter as a function of wood species and combustion condition. J Hazard Mater. 2023;441:129874.
26. Kelesidis GA, Goudeli E, Pratsinis SE. Morphology and mobility diameter of carbonaceous aerosols during agglomeration and surface growth. Carbon. 2017;121:527–35.
27. Beltran-Huarac J, Zhang Z, Pyrgiotakis G, DeLoid G, Vaze N, Demokritou P. Development of reference metal and metal oxide engineered nanomaterials for nanotoxicology research using high throughput and precision flame spray synthesis approaches. NanoImpact. 2018;10:26–37.
28. DeCarlo PF, Slowik JG, Worsnop DR, Davidovits P, Jimenez JL. Particle morphology and density characterization by combined mobility and aerodynamic diameter measurements. Part 1: theory. Aerosol Sci Technol. 2004;38:1185–205.
29. Schmid O, Karg E, Hagen DE, Whitefield PD, Ferron GA. On the effective density of non-spherical particles as derived from combined measurements of aerodynamic and mobility equivalent size. J Aerosol Sci. 2007;38:431–43.
30. Spyrogianni A, Karadima KS, Goudeli E, Mavrantzas VG, Pratsinis SE. Mobility and settling rate of agglomerates of polydisperse nanoparticles. J Chem Phys. 2018;148:064703.
31. Demokritou P, Gass S, Pyrgiotakis G, Cohen JM, Goldsmith W, McKinney W, Frazer D, Ma J, Schwegler-Berry D, Brain J. An in vivo and in vitro toxicological characterisation of realistic nanoscale CeO_2 inhalation exposures. Nanotoxicology. 2013;7:1338–50.
32. Cohen JM, DeLoid GM, Demokritou P. A critical review of in vitro dosimetry for engineered nanomaterials. Nanomedicine. 2015;10:3015–32.
33. Asgharian B, Price O, Oldham M, Chen L-C, Saunders E, Gordon T, Mikheev VB, Minard KR, Teeguarden JG. Computational modeling of nanoscale and microscale particle deposition, retention and dosimetry in the mouse respiratory tract. Inhal Toxicol. 2014;26:829–42.
34. Anjilvel S, Asgharian B. A multiple-path model of particle deposition in the rat lung. Fundam Appl Toxicol. 1995;28:41–50.
35. Human respiratory tract model for radiological protection. A report of a task group of the international commission on radiological protection. Ann ICRP. 1994;24:1–482.

36. Oh H-J, Min Y, Kim J. Exposure to long-range transported particulate matter and modeling age-related particle deposition. Environ Sci Pollut. 2021;28:69286–300.
37. Wang H, Yin P, Fan W, Wang Y, Dong Z, Deng Q, Zhou M. Mortality risk associated with short-term exposure to particulate matter in China: estimating error and implication. Environ Sci Technol. 2020;55:1110–21.
38. Man R, Wu Z, Zong T, Voliotis A, Qiu Y, Größ J, van Pinxteren D, Zeng L, Herrmann H, Wiedensohler A. Impact of water uptake and mixing state on submicron particle deposition in the human respiratory tract (HRT) based on explicit hygroscopicity measurements at HRT-like conditions. Atmospheric Chem Phys. 2022;22:12387–99.
39. Qiu Z, Wang X, Liu Z, Luo J. Quantitative assessment of cyclists' exposure to PM and BC on different bike lanes. Atmospheric Pollut Res. 2022;13:101588.
40. Hammer T, Gao H, Pan Z, Wang J. Relationship between aerosols exposure and lung deposition dose. Aerosol Air Qual Res. 2020;20:1083–93.
41. Hammer T, Fissan H, Wang J. Determination of the delivered dose of nanoparticles in the trachea-bronchial and alveolar regions of the lung. NanoImpact. 2019;14:100162.
42. Ling M-P, Chio C-P, Chou W-C, Chen W-Y, Hsieh N-H, Lin Y-J, Liao C-M. Assessing the potential exposure risk and control for airborne titanium dioxide and carbon black nanoparticles in the workplace. Environ Sci Pollut. 2011;18:877–89.
43. Dekkers S, Ma-Hock L, Lynch I, Russ M, Miller MR, Schins RP, Keller J, Römer I, Küttler K, Strauss V. Differences in the toxicity of cerium dioxide nanomaterials after inhalation can be explained by lung deposition, animal species and nanoforms. Inhal Toxicol. 2018;30:273–86.
44. Cary CM, Seymore TN, Singh D, Vayas KN, Goedken MJ, Adams S, Polunas M, Sunil VR, Laskin DL, Demokritou P. Single inhalation exposure to polyamide micro and nanoplastic particles impairs vascular dilation without generating pulmonary inflammation in virgin female Sprague Dawley rats. Part Fibre Toxicol. 2023;20:1–14.
45. Pal AK, Watson CY, Pirela SV, Singh D, Chalbot M-CG, Kavouras I, Demokritou P. Linking exposures of particles released from nano-enabled products to toxicology: an integrated methodology for particle sampling, extraction, dispersion, and dosing. Toxicol Sci. 2015;146:321–33.
46. Pirela SV, Bhattacharya K, Wang Y, Zhang Y, Wang G, Christophi CA, Godleski J, Thomas T, Qian Y, Orandle MS. A 21-day sub-acute, whole-body inhalation exposure to printer-emitted engineered nanoparticles in rats: exploring pulmonary and systemic effects. NanoImpact. 2019;15:100176.
47. Pirela SV, Lu X, Miousse I, Sisler JD, Qian Y, Guo N, Koturbash I, Castranova V, Thomas T, Godleski J. Effects of intratracheally instilled laser printer-emitted engineered nanoparticles in a mouse model: a case study of toxicological implications from nanomaterials released during consumer use. NanoImpact. 2016;1:1–8.
48. Avino P, Scungio M, Stabile L, Cortellessa G, Buonanno G, Manigrasso M. Second-hand aerosol from tobacco and electronic cigarettes: Evaluation of the smoker emission rates and doses and lung cancer risk of passive smokers and vapers. Sci Total Environ. 2018;642:137–47.
49. DeLoid GM, Cohen JM, Pyrgiotakis G, Demokritou P. Preparation, characterization, and in vitro dosimetry of dispersed, engineered nanomaterials. Nat Protoc. 2017;12:355–71.
50. DeLoid GM, Cohen JM, Darrah T, Derk R, Rojanasakul L, Pyrgiotakis G, Wohlleben W, Demokritou P. Estimating the effective density of engineered nanomaterials for in vitro dosimetry. Nat Commun. 2014;5:3514.
51. Wierzbicka A, Nilsson PT, Rissler J, Sallsten G, Xu Y, Pagels JH, Albin M, Österberg K, Strandberg B, Eriksson A. Detailed diesel exhaust characteristics including particle surface area and lung deposited dose for better understanding of health effects in human chamber exposure studies. Atmospheric Environ. 2014;86:212–9.
52. Ehara K, Hagwood C, Coakley KJ. Novel method to classify aerosol particles according to their mass-to-charge ratio—aerosol particle mass analyser. J Aerosol Sci. 1996;27:217–34.
53. Charvet A, Bau S, Paez Coy NE, Bémer D, Thomas D. Characterizing the effective density and primary particle diameter of airborne nanoparticles produced by spark discharge using mobility and mass measurements (tandem DMA/APM). J Nanopart Res. 2014;16:1–11.
54. Wang J, Bahk YK, Chen S-C, Pui DY. Characteristics of airborne fractal-like agglomerates of carbon nanotubes. Carbon. 2015;93:441–50.
55. Park K, Cao F, Kittelson DB, McMurry PH. Relationship between particle mass and mobility for diesel exhaust particles. Environ Sci Technol. 2003;37:577–83.
56. Kelesidis GA, Pratsinis SE. Determination of the volume fraction of soot accounting for its composition and morphology. Proc Combust Inst. 2021;38:1189–96.
57. Olfert J, Symonds J, Collings N. The effective density and fractal dimension of particles emitted from a light-duty diesel vehicle with a diesel oxidation catalyst. J Aerosol Sci. 2007;38:69–82.
58. Kim SH, Zachariah MR. In-flight kinetic measurements of the aerosol growth of carbon nanotubes by electrical mobility classification. J Phys Chem B. 2006;110:4555–62. https://doi.org/10.1021/jp0541718.
59. Kim SH, Mulholland GW, Zachariah MR. Density measurement of size selected multiwalled carbon nanotubes by mobility-mass characterization. Carbon. 2009;47:1297–302.
60. Maricq MM, Xu N. The effective density and fractal dimension of soot particles from premixed flames and motor vehicle exhaust. J Aerosol Sci. 2004;35:1251–74.
61. Hering SV, Stolzenburg MR. On-line determination of particle size and density in the nanometer size range. Aerosol Sci Technol. 1995;23:155–73.
62. Spencer MT, Shields LG, Prather KA. Simultaneous measurement of the effective density and chemical composition of ambient aerosol particles. Environ Sci Technol. 2007;41:1303–9.
63. Oberdörster G, Kuhlbusch TA. In vivo effects: Methodologies and biokinetics of inhaled nanomaterials. NanoImpact. 2018;10:38–60.
64. Leskinen J, Ihalainen M, Torvela T, Kortelainen M, Lamberg H, Tiitta P, Jakobi G, Grigonyte J, Joutsensaari J, Sippula O. Effective density and morphology of particles emitted from small-scale combustion of various wood fuels. Environ Sci Technol. 2014;48:13298–306.
65. Rissler J, Swietlicki E, Bengtsson A, Boman C, Pagels J, Sandström T, Blomberg A, Löndahl J. Experimental determination of deposition of diesel exhaust particles in the human respiratory tract. J Aerosol Sci. 2012;48:18–33.
66. Momenimovahed A, Olfert J. Effective density and volatility of particles emitted from gasoline direct injection vehicles and implications for particle mass measurement. Aerosol Sci Technol. 2015;49:1051–62.
67. Quiros DC, Hu S, Hu S, Lee ES, Sardar S, Wang X, Olfert JS, Jung HS, Zhu Y, Huai T. Particle effective density and mass during steady-state operation of GDI, PFI, and diesel passenger cars. J Aerosol Sci. 2015;83:39–54.
68. Trivanovic U, Corbin JC, Baldelli A, Peng W, Yang J, Kirchen P, Miller JW, Lobo P, Gagné S, Rogak SN. Size and morphology of soot produced by a dual-fuel marine engine. J Aerosol Sci. 2019;138:105448.
69. Wang M, Mei J, You X. Effect of potassium chloride addition on soot formation during ethylene pyrolysis in a flow reactor. Combust Flame. 2021;223:118–26.
70. Kelesidis GA, Furrer FM, Wegner K, Pratsinis SE. Impact of humidity on silica nanoparticle agglomerate morphology and size distribution. Langmuir. 2018;34:8532–41.
71. Goudeli E, Gröhn AJ, Pratsinis SE. Sampling and dilution of nanoparticles at high temperature. Aerosol Sci Technol. 2016;50:591–604.
72. Kelesidis GA, Goudeli E, Pratsinis SE. Flame synthesis of functional nanostructured materials and devices: surface growth and aggregation. Proc Combust Inst. 2017;36:29–50.
73. Kelesidis GA, Pratsinis SE. Soot light absorption and refractive index during agglomeration and surface growth. Proc Combust Inst. 2019;37:1177–84.
74. Kelesidis GA, Bruun CA, Pratsinis SE. The impact of organic carbon on soot light absorption. Carbon. 2021;172:742–9.
75. Kelesidis GA, Kholghy MR, Zuercher J, Robertz J, Allemann M, Duric A, Pratsinis SE. Light scattering from nanoparticle agglomerates. Powder Technol. 2020;365:52–9.
76. Kelesidis GA, Crepaldi P, Allemann M, Duric A, Pratsinis SE. The mobility diameter of soot determines its angular light scattering distribution. Combust Flame. 2022:112476.
77. Kelesidis GA, Neubauer D, Fan L-S, Lohmann U, Pratsinis SE. Enhanced light absorption and radiative forcing by black carbon agglomerates. Environ Sci Technol. 2022;56:8610–8.
78. Kelesidis GA, Nagarkar A, Trivanovic U, Pratsinis SE. Toward elimination of soot emissions from jet fuel combustion. Environ Sci Technol. 2023;57:10276–83.

79. Olfert J, Rogak S. Universal relations between soot effective density and primary particle size for common combustion sources. Aerosol Sci Technol. 2019;53:485–92.
80. Hinds WC, Zhu Y. Aerosol technology: properties, behavior, and measurement of airborne particles. Wiley; 2022.
81. Taulbee DB, Yu C. A theory of aerosol deposition in the human respiratory tract. J Appl Physiol. 1975;38:77–85.
82. Hofmann W, Golser R, Balashazy I. Inspiratory deposition efficiency of ultrafine particles in a human airway bifurcation model. Aerosol Sci Technol. 2003;37:988–94.
83. Cheng YS. Aerosol deposition in the extrathoracic region. Aerosol Sci Technol. 2003;37:659–71.
84. Trivanovic U, Kelesidis GA, Pratsinis SE. High-throughput generation of aircraft-like soot. Aerosol Sci Technol. 2022;56:732–43.
85. Trivanovic U, Martins MP, Benz S, Kelesidis GA, Pratsinis SE. Dynamics of soot surface growth and agglomeration by enclosed spray combustion of jet fuel. Fuel. 2023;342:127864.
86. Eggersdorfer ML, Gröhn AJ, Sorensen C, McMurry PH, Pratsinis SE. Mass-mobility characterization of flame-made ZrO_2 aerosols: primary particle diameter and extent of aggregation. J Colloid Interface Sci. 2012;387:12–23.
87. Sipkens TA, Boies A, Corbin JC, Chakrabarty RK, Olfert J, Rogak SN. Overview of methods to characterize the mass, size, and morphology of soot. J Aerosol Sci. 2023;173:106211.
88. McMurry PH, Wang X, Park K, Ehara K. The relationship between mass and mobility for atmospheric particles: a new technique for measuring particle density. Aerosol Sci Technol. 2002;36:227–38.
89. Price O, Asgharian B, Miller F, Cassee F, de Winter-Sorkina R. Multiple Path Particle Dosimetry model (MPPD v1. 0): a model for human and rat airway particle dosimetry. RIVM rapport 650010030. 2002.
90. Asgharian B, Hofmann W, Bergmann R. Particle deposition in a multiple-path model of the human lung. Aerosol Sci Technol. 2001;34:332–9.
91. Yeh H-C, Schum G. Models of human lung airways and their application to inhaled particle deposition. Bull Math Biol. 1980;42:461–80.
92. Martin J, Bello D, Bunker K, Shafer M, Christiani D, Woskie S, Demokritou P. Occupational exposure to nanoparticles at commercial photocopy centers. J Hazard Mater. 2015;298:351–60.
93. Gross EA, Swenberg JA, Fields S, Popp J. Comparative morphometry of the nasal cavity in rats and mice. J Anat. 1982;135:83.
94. Guyton AC. Measurement of the respiratory volumes of laboratory animals. Am J Physiol Legacy. 1947;150:70–7.
95. Piccione G, Caola G, Mortola JP. Scaling the daily oscillations of breathing frequency and skin temperature in mammals. Comp Biochem Physiol Part A Mol Integr Physiol. 2005;140:477–86.
96. De Vleeschauwer SI, Rinaldi M, De Vooght V, Vanoirbeek JA, Vanaudenaerde BM, Verbeken EK, Decramer M, Gayan-Ramirez GN, Verleden GM, Janssens W. Repeated invasive lung function measurements in intubated mice: an approach for longitudinal lung research. Lab Anim. 2011;45:81–9.
97. Jew K, Herr D, Wong C, Kennell A, Morris-Schaffer K, Oberdörster G, O'Banion MK, Cory-Slechta DA, Elder A. Selective memory and behavioral alterations after ambient ultrafine particulate matter exposure in aged 3xTgAD Alzheimer's disease mice. Part Fibre Toxicol. 2019;16:1–17.
98. Herr D, Jew K, Wong C, Kennell A, Gelein R, Chalupa D, Raab A, Oberdörster G, Olschowka J, O'Banion MK. Effects of concentrated ambient ultrafine particulate matter on hallmarks of Alzheimer's disease in the 3xTgAD mouse model. Neurotoxicology. 2021;84:172–83.
99. Glaab T, Daser A, Braun A, Neuhaus-Steinmetz U, Fabel H, Alarie Y, Renz H. Tidal midexpiratory flow as a measure of airway hyperresponsiveness in allergic mice. Am J Physiol Cell Physiol. 2001;280:L565–73.
100. EPA: National Ambient Air Quality Standards (NAAQS) for PM. https://www.epa.gov/pm-pollution/national-ambient-air-quality-standards-naaqs-pm (2023). Accessed May 15 2023.
101. Zhang J, Fan X, Graham L, Chan TW, Brook JR. Evaluation of an annular denuder system for carbonaceous aerosol sampling of diesel engine emissions. J Air Waste Manag Assoc. 2013;63:87–99. https://doi.org/10.1080/10962247.2012.739582.
102. Jonsdottir HR, Delaval M, Leni Z, Keller A, Brem BT, Siegerist F, Schönenberger D, Durdina L, Elser M, Burtscher H. Non-volatile particle emissions from aircraft turbine engines at ground-idle induce oxidative stress in bronchial cells. Commun Biol. 2019;2:90.

Publisher's Note